

Unpaired Topological Triply Degenerate Point for Spin-Tensor-Momentum-Coupled Ultracold Atoms

Zhoutao Lei,^{1,2} Yuangang Deng,^{1,*} and Chaohong Lee^{1,2,3,†}

¹*Guangdong Provincial Key Laboratory of Quantum Metrology and Sensing & School of Physics and Astronomy, Sun Yat-Sen University (Zhuhai Campus), Zhuhai 519082, China*

²*State Key Laboratory of Optoelectronic Materials and Technologies, Sun Yat-Sen University (Guangzhou Campus), Guangzhou 510275, China*

³*Synergetic Innovation Center for Quantum Effects and Applications, Hunan Normal University, Changsha 410081, China*

(Dated: December 7, 2021)

The realization of triply degenerated points (TDPs) with exotic fermionic excitations have opened a new perspective for understanding of our nature. Here we propose an experimental scheme to realize novel three dimensional topological semimetals including the types of single unpaired TDP and multiple two-fold Weyl points (WPs) for ultracold pseudospin-1 atomic gases trapped in optical lattices. Compared to the earlier studies, the predicted single unpaired TDP emerged by the interplay of quadratic spin-vector- and spin-tensor-momentum-coupling contains a topological nontrivial middle band. Strikingly, the topologically protected Fermi-arcs states linking the single unpaired TDP and one (two) WPs have appeared, in contrast to conventional TDPs that Fermi arcs connect the same degeneracies of band degenerate points with opposite chirality. Furthermore, the different types of TDPs can be distinguished through the unique linking structure of Fermi arcs. Our scheme may provide a platform for emerging exotic quasiparticle excitations of fermions in cold atoms.

Introduction.—Topological semimetal is a kind of gapless topological phase of matter which exhibits band degenerate point (BDP) in momentum space and supports topologically protected Fermi arc surface states on the boundary of its bulk sample [1]. The Weyl (Dirac) semimetal [2–4] acts as a paradigm that hosts pairs of two-fold (four-fold) linear BDPs. The excitations near these two types of BDPs provide analogs of relativistic fermions with half-integer spins in quantum field theory. Unlike Weyl points (WPs) carrying singly quantized topological charge, Dirac points can be treated as the overlap of two WPs with opposite chirality. Interestingly, these novel quasiparticle excitations of fermions not only play important roles for exploration of fundamental physics but also provide versatile practical applications including large negative magnetoresistance [5, 6], anomalous Hall conductivity [7, 8], and nontrivial quantum oscillation signatures [9–11].

Besides the experimentally realized two- and four-fold BDPs for half-integer spin particles [12–20], the new types of topological BDPs with different degeneracies have been studied [21, 22]. Remarkably, the triply degenerate point (TDP), which represents a new type of quasiparticle for integer pseudospins with no high-energy counterparts [21, 22], has been experimental observed in various quantum systems, such as solid states [23, 24], phononic crystal [25], and superconducting qutrit [26]. In general, the typical Hamiltonian of TDPs is making up of the linear order of spin-vector-momentum coupling (SVMC), e.g., $H = \mathbf{q} \cdot \mathbf{F}$, where \mathbf{q} is the momentum deviation from the TDPs and \mathbf{F} is the spin-1 matrix. Moreover, recent advances demonstrate that a quadratic dispersion along two directions of momentum

space could generate double-triple-point for spin-1 quantum gases [27]. These aforementioned TDPs appear in pairs which carry opposite topological charges due to the ‘no-go’ theorem [28, 29] and host a topological trivial middle band as well.

Meanwhile, a different type of spin-tensor-momentum coupling (STMC) can be constructed in high-spin ultracold atoms, which could offer opportunities for exploring new topological quantum matters in a highly controllable way [30–38]. Based on the capability in current experiments of spin-orbit coupling (SOC) [39–42] and Raman-assisted tunneling in optical lattices [43–48], it is of great interest to explore *whether single unpaired TDP corresponding the exotic topologically protected Fermi-arcs states can be realized*. An affirmative answer will open up unprecedented opportunities for exploring basic science and provide a broad physics community of applications in designing new generations of quantum devices [5–11].

In this Letter, we propose an experimental scheme to realize novel TDPs for ultracold pseudospin-1 atomic gases trapped in a cubic optical lattice. We show that the system exhibits different types of TDPs, including a single unpaired unconventional TDP hosting nontrivial middle band emerged by quadratic SVMC and STMC. In addition, several two-fold WPs appear in our system, which provides a controllable platform to explore the co-existence of multiple types of topological fermions [49–57]. Remarkably, the exotic Fermi arcs connecting TDP and WPs are observed. Furthermore, we demonstrate that the generated different types of TDPs can be unambiguously distinguished through the spin-resolved of time-of-flight images in experiments [41, 58, 59].

Model.—We consider an ultracold gas of N fermionic

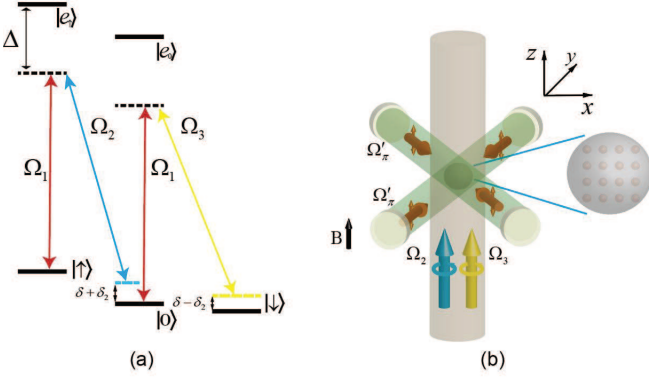


Figure 1. (color online). (a) Level diagram. (b) Laser configurations of generating quadratic SVMC and STMC.

atoms subjected to a bias magnetic field \mathbf{B} along the quantization z axis. The atomic level structure is shown in Fig. 1(a), where five relevant magnetic Zeeman sub-levels with three ground states and two electronic excited states are involved. Take ^{40}K as an example [36], the atomic transition from the ground state $|\sigma\rangle$ ($\sigma = \{\uparrow, 0\}$) to the excited state $|e_\sigma\rangle$ is driven by pair of π -polarized standing-wave lasers with Rabi frequencies $\Omega'_\pi \sin(k_L x - k_L y)$ and $i\Omega'_\pi \sin(k_L x + k_L y)$ as shown in Fig. 1(b), where k_L is the wave vector of laser with the lattice constant $a = \pi/k_L$. Then the total Rabi frequency $\Omega_1(\mathbf{r}) = \Omega_\pi[\sin(k_L x) \cos(k_L y) + i \cos(k_L x) \sin(k_L y)]$ is generated with $\Omega_\pi = \sqrt{2}e^{i\pi/4}\Omega'_\pi$ [60]. To generate SOC, the atomic transition $|0\rangle \leftrightarrow |e_\uparrow\rangle$ and $|e_0\rangle \leftrightarrow |\downarrow\rangle$ are driven by σ -polarized plane-wave lasers propagating along z -direction with the same Rabi frequency $\Omega_2(\mathbf{r}) = \Omega_3(\mathbf{r})$ (see Supplemental Materials (SM) [61]), where the frequency difference between two lasers can be used to compensated the quadratic Zeeman shift. For the large atom-light detuning Δ , two excited states can be safely adiabatically eliminated to yield the pseudospin-1 system.

In the tight-binding regime, the lattice Hamiltonian in momentum space takes the form [61]

$$H_0(\mathbf{k}) = \sum_{\alpha=x,y,z} d_\alpha(\mathbf{k})\hat{F}_\alpha + d'_z(\mathbf{k})\hat{F}_z^2 + \epsilon(\mathbf{k})\hat{I}, \quad (1)$$

where $\mathbf{k} = (k_x, k_y, k_z)$ is in the first Brillouin zone (BZ), $d_x(\mathbf{k}) = 2t_0 \sin(k_x a)$, $d_y(\mathbf{k}) = 2t_0 \sin(k_y a)$, $d_z(\mathbf{k}) = \delta - t_1 \sin(k_z a)$, $d'_z(\mathbf{k}) = \delta_2 - 4t \cos(k_x a) - 4t \cos(k_y a) - t_2 \cos(k_z a)$ and $\epsilon(\mathbf{k}) = 2t \cos(k_x a) + 2t \cos(k_y a) - 2t \cos(k_z a)$. Here δ (δ_2) is the effective tunable linear (quadratic) Zeeman shift, t_0 is Raman-assisted spin-flip hopping, and t is spin-independent hopping with $t_1 = 2t \sin(\sqrt{2}\pi)$ and $t_2 = 2t[\cos(\sqrt{2}\pi) - 1]$. Obviously, the first term $d_\alpha(\mathbf{k})\hat{F}_\alpha$ represent the conventional SVMC and the second term $d'_z(\mathbf{k})\hat{F}_z^2$ denotes the interesting STMC for our high-spin system.

Remarkably, the Hamiltonian (1) possesses a four-fold rotation symmetry around z axis $\mathcal{C}_{4z}H_0(k_x, k_y, k_z)\mathcal{C}_{4z}^{-1} =$

$H_0(-k_y, k_x, k_z)$ with $\mathcal{C}_{4z} = e^{-i\pi/2\hat{F}_z}$. As a result, the emerged BDPs will be appeared at high-symmetry lines due to \mathcal{C}_{4z} symmetry. After ignoring the identity term of $\epsilon(\mathbf{k})\hat{I}$, the interplay of SVMC of $d_z(\mathbf{k})\hat{F}_z$ and STMC of $d'_z(\mathbf{k})\hat{F}_z^2$ will break mirror symmetry, which is necessary to guarantee a single unpaired TDP. In fact, the separate term of SVMC and STMC is satisfying the different mirror symmetry with $H_0(k_x, k_y, k_z) = H_0(k_x, k_y, \pi - k_z)$ and $H_0(k_x, k_y, k_z) = H_0(k_x, k_y, -k_z)$, respectively. For simplicity, we set $t_0 = t$ since the topological phase boundaries is independent of nonzero t_0/t . Thus the free parameters in our model reduce to the tunable linear Zeeman shift δ and quadratic Zeeman shift δ_2 .

Triply Degenerate Point.—To investigate the system topologies, we calculate energy spectrum by diagonalizing Hamiltonian (1). The three energy bands can be obtained corresponding the eigenstate $|\psi_n(\mathbf{k})\rangle$ and eigenenergy E_n with $n = \pm 1, 0$ denoting indices of n th band. In contrast to the previously studies [23–27] that the TDPs appear in pairs (e.g., located at $\mathbf{K}_+ = (0, 0, k_0)$ and $\mathbf{K}_- = (0, 0, \pi/a - k_0)$) with opposite chirality under the ‘no-go’ theorem [28, 29], we emphasize that the generated single TDP in our model is unpaired due to the mirror symmetry breaking. It can be shown that the single unpaired TDP is located at momentum $\mathbf{K} = (0, 0, k_0)$ when the linear and quadratic Zeeman fields are satisfying $\delta = t_1 \sin(k_0 a)$ and $\delta_2 = 8t + t_2 \cos(k_0 a)$, simultaneously. Then the effective TDP Hamiltonian with expanding Eq. (1) in the vicinity of \mathbf{K} , takes the form

$$H(\mathbf{q}) = \sum_{\alpha=x,y} v_\alpha q_\alpha \hat{F}_\alpha + (v_z q_z + v'_z q_z^2) \hat{F}_z + (u_z q_z + u'_z q_z^2) \hat{F}_z^2 + v_0(\mathbf{q}) \hat{I}, \quad (2)$$

where \mathbf{q} indicates the wave vector with respect to \mathbf{K} , $v_x = v_y = 2t_0 a$, $v_z = -t_1 \cos(k_0 a) a$, $u_z = t_2 \sin(k_0 a) a$, $v'_z = (t_1/2t_2) a u_z$, $u'_z = -(t_2/2t_1) a v_z$, and $v_0(\mathbf{q}) = 4t - 2t \cos(k_0 a) + 2t \sin(k_0 a) q_z a$. Remarkably, the different types of SOC are generated in our model. Besides the linear dispersion along q_z axis, both the quadratic dispersion of SVMC and STMC terms are emerged. Here, the linear and quadratic Zeeman fields can be treated as the control knobs for SOC strengths v_z , u_z , v'_z and u'_z .

In general, the quantized topological charge of TDP can be characterized by the first Chern number

$$\mathcal{C}_n = \frac{1}{2\pi} \oint_{\mathbf{S}} \boldsymbol{\Omega}_n \cdot d\mathbf{S}, \quad (3)$$

where \mathbf{S} indicates a closed surface enclosing TDP and $\boldsymbol{\Omega}_n(\mathbf{k}) = \nabla_{\mathbf{k}} \times \langle \psi_n(\mathbf{k}) | i \nabla_{\mathbf{k}} | \psi_n(\mathbf{k}) \rangle$ is the Berry curvature of n th band.

Phase Diagram.—Figure 2(a) summarize the phases diagram of TDP in the v_z - u_z parameter plane, where each distinct TDP phase is characterized by Chern number configuration, i.e., $\{\mathcal{C}_{-1}, \mathcal{C}_0, \mathcal{C}_1\}$. As can be seen, the Chern number for the n th band is $\mathcal{C}_n = -2n v_z / |v_z|$ when

the SOC strengths in Eq. (2) satisfy $|v_z/u_z| > 1$. While for $|u_z/v_z| > 1$, the Chern number for the n th band is satisfying $C_n = -nv_z/|v_z|$, which result is analogous to generation of topological TDPs induced by STMC [33]. We should note that the SOC strength of v_z and u_z are highly controlled by δ and δ_2 .

To process further, we use the Chern number of lowest band to characterize the topological charge of TDP, i.e., $C = C_{-1}$. Therefore the single unpaired TDP carries doubly (singly) topological charge with $C = \pm 2$ ($C = \pm 1$) in the region $|v_z/u_z| > 1$ ($|u_z/v_z| > 1$). In Fig. 2(b) and 2(c), we plot the typical band spectra for doubly and singly TDP phase, respectively. We show that the middle band of conventional TDPs are topological trivial with $C_0 = 0$. This result can be understood as follows. The quadratic terms in Hamiltonian (2) does not influence the band closing and opening of bulk gap when $|u_z/v_z| \neq 1$ and $v_z \neq 0$, which indicates the system topology is captured by an effective Hamiltonian with only including linear terms, $\tilde{H}(\mathbf{q}) = \sum_{\alpha=x,y,z} v_\alpha q_\alpha \hat{F}_\alpha + u_z q_z \hat{F}_z^2$. This Hamiltonian $\tilde{H}(\mathbf{q})$ preserves a linear relation dependence of the momenta with $\tilde{H}(\mathbf{q}) = -\tilde{H}(-\mathbf{q})$. Thus the Berry curvature is constrained by the relation $\Omega_n(\mathbf{q}) = \Omega_{-n}(-\mathbf{q})$, which will yield zero topological charge for middle band with $C_0 = 0$ and $C_{-1} = -C_1$.

Compared with conventional TDPs, we find other three types of unpaired topological TDPs with hosting topological nontrivial middle band ($C_0 \neq 0$) at $v_z = \pm u_z$ or $v_z = 0$ [dashed lines in Fig. 2(a)]. To further characterize these phases, we plot the typical energy spectra $E(\mathbf{q})$ for two of them, as shown in Figs. 2(d) and 2(e). We emphasize that the predicted unconventional TDPs with $C_0 \neq 0$ are induced by the interplay of quadratic SVMC and STMC. Explicitly, the quadratic SVMC ($v'_z q_z^2 \hat{F}_z$) breaks the relation $\tilde{H}(\mathbf{q}) = -\tilde{H}(-\mathbf{q})$ at the boundary of topological phase transitions, which yields $C_{-1} \neq -C_1$. Then the topological nontrivial middle band with nonzero Chern number can be expected since $\sum_n C_n = 0$. For absent the STMC ($u_z q_z \hat{F}_z^2$), we find that the TDP will reduce to a topological trivial point which can be treated as combination of a pair of topological nontrivial TDPs with opposite topological charge.

Fermi Arcs of TDPs.—Besides the existing unconventional and conventional unpaired topological TDPs, two types of two-fold WPs with different topological charge are observed in band structures. Figs. 3(a)-3(d) shows the energy spectrum for different TDP phases along high-symmetry line with $k_x = k_y = 0$. It is showing that three and two WPs as well as single unpaired conventional and unconventional TDP are appeared in the first BZ, respectively. Furthermore, we plot the Berry curvature of lowest band Ω_{-1} for the four types of TDP phases in the k_z - k_x plane, as shown in Figs. 3(e)-3(h). The topological charge of WPs can be well defined by the lower touching band topology. Here, two-fold BDPs with singly

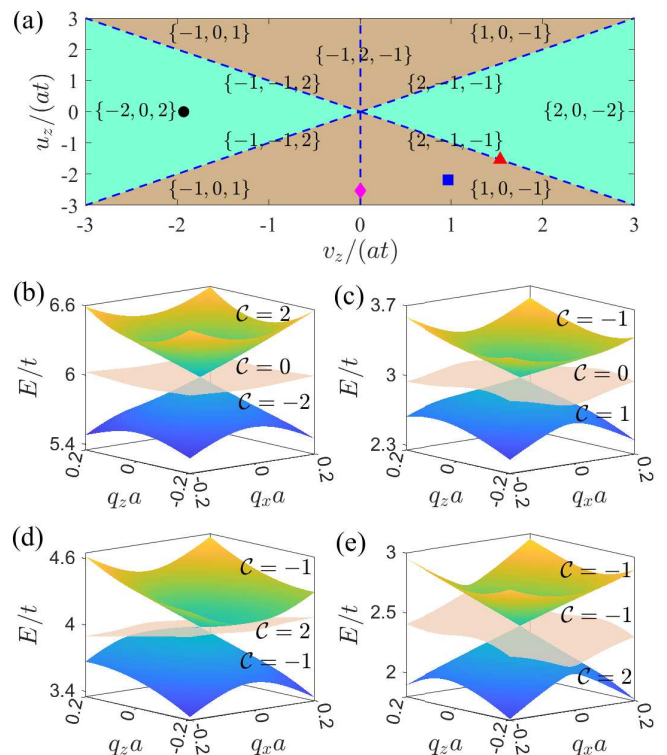


Figure 2. (color online). (a) The phase diagram of TDP in v_z - u_z parameter plane. (b)-(e) The energy dispersion near TDP as a function of q_x and q_z with $q_y = 0$ for different phases. The black circle and blue square (magenta diamond and red triangle) in (a) mark the parameters for (b) and (c) [(d) and (e)], corresponding to conventional (unconventional) TDP phases.

($C = \pm 1$) and doubly ($C = \pm 2$) topological charge is called singly WPs and doubly WPs, respectively. The emergence of two-fold WPs can be characterized by an effective two-band Hamiltonian as discussed in SM [61]. As can be seen, TDP or WPs with positive (negative) Chern number displays as a source (sink) of Berry curvature, which unambiguously demonstrates its nontrivial topological properties. We also check that the total topological charge of all BDPs for the n th energy band in the first BZ is zero, e.g., $\sum_{BDP_s} C_{-1} = 0$ [28, 29].

To gain more insight into topological TDPs, we explore the topological protected Fermi arcs which are the surface states crossing the Fermi energy. Figs. 3(i)-3(l) display the typical surface spectra density for different types of TDPs on the $(0\bar{1}0)$ surface by using the recursive Green's function method [61, 62]. Compared to earlier realization of TDPs appearing in pairs [23-27], the emerged single topological TDP is unpaired due to mirror symmetry breaking. Interestingly, the Fermi arcs states will link single TDP and two-fold WPs in our model. It can be shown that each TDP phase corresponding the unique linking structures of Fermi arcs is observed.

Specifically, the number of Fermi arcs linking to single

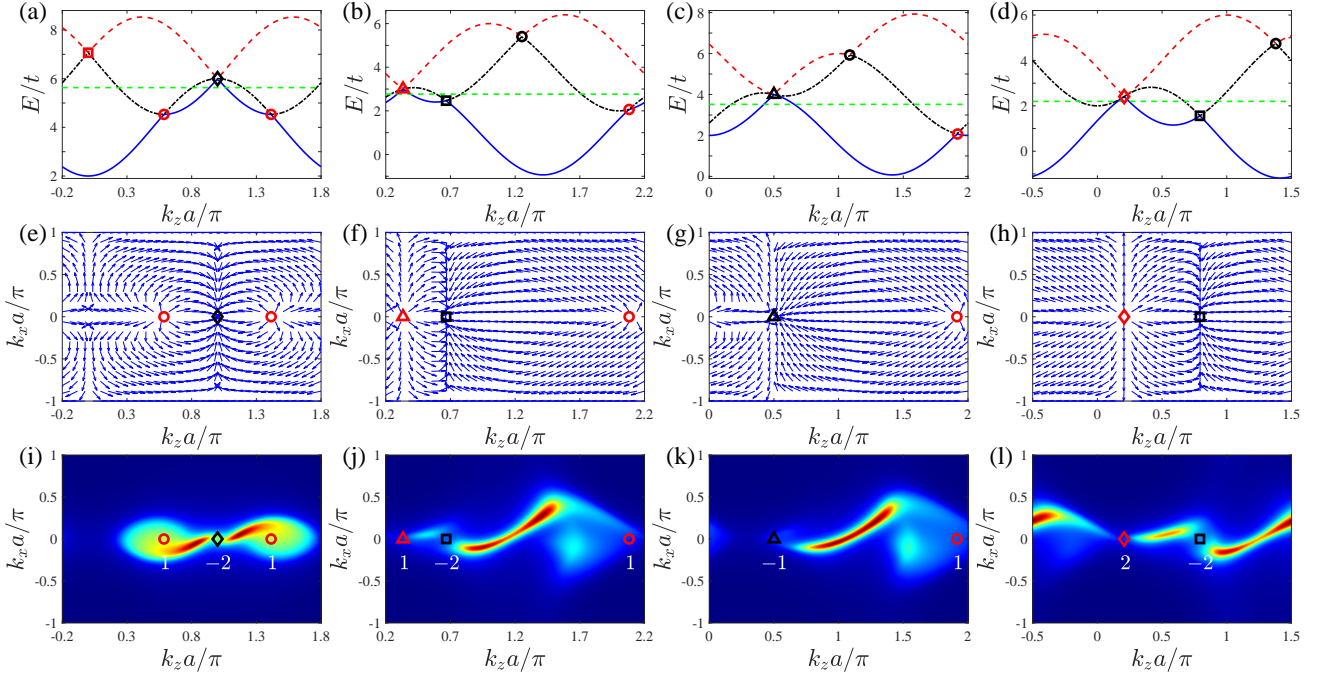


Figure 3. (color online). (a)-(d) The energy dispersion along high-symmetry line $k_x = k_y = 0$ for the same parameters as in Figs. 2(b)-2(e), respectively. (e-h) The corresponding in-plane Berry curvature of lowest band Ω_{-1} in $k_y = 0$ plane. (i-l) The corresponding surface spectral density on the $(0\bar{1}0)$ surface with Fermi energy shown as green dashed line in (a-d) respectively. Here the red- (black-) circle (square) and triangle (diamond) denotes the singly (doubly) WPs and TDP with a positive (negative) topological charge, respectively. The white numbers represent topological charge of BDPs.

TDP is determined by its quantized topological charge \mathcal{C} . Moreover, the Fermi arcs are directly linked single TDP and two (one) WPs for conventional (unconventional) TDP phases, as shown in Figs. 3(i) and 3(j) [Figs. 3(k) and 3(l)]. It is shown that conventional TDP with $\mathcal{C} = -2$ and $\mathcal{C} = 1$ are both exhibiting two separate Fermi arcs with three nodes. In fact, the unconventional TDP can be treated as the combination of one conventional TDP and one WP [61], which could provide a new insight into unconventional TDP with topological non-trivial middle band. Of particular interest, the unconventional TDP with singly (doubly) topological charge is connected to one WPs with opposite chirality and hosts one (two) Fermi arcs as well, as displayed in Fig. 3(k) [Fig. 3(l)]. Remarkably, the observed novel Fermi arcs act as the unique surface fingerprints for different types of TDPs.

Determination of TDPs.—In order to further reveal topology of TDP, we calculate spin textures for different TDPs. Remarkably, the eigenstates of the helicity branches for Hamiltonian (1) are always reduced to the bare spin states at high-symmetry line $k_x = k_y = 0$ due to \mathcal{C}_{4z} symmetry. These properties provide a unique opportunity to experimental measurement of Chern number of single unpaired TDP through spin-resolved TOF images [41, 58, 59]. Fig. 4 shows the typical spin texture around the four types of TDP phases at $k_x = k_y = 0$. As

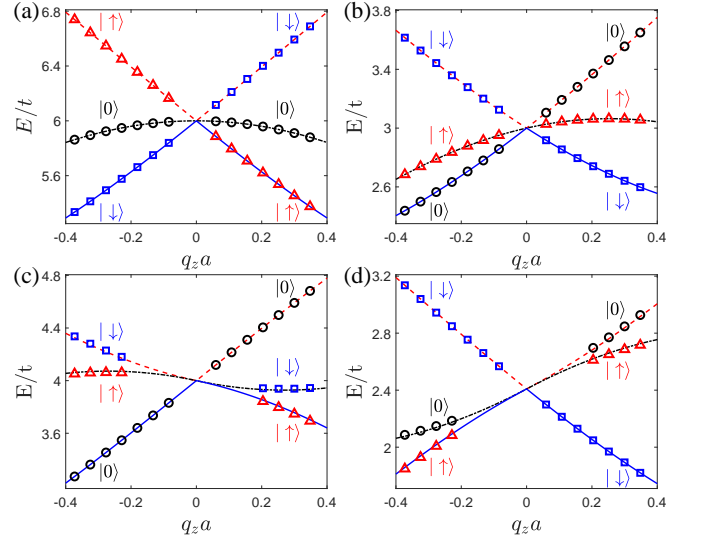


Figure 4. (color online). The spin texture of different energy bands near TDP along $k_x = k_y = 0$ for spin- \uparrow (Δ), spin-0 (\circ), and spin- \downarrow (\square). The parameters are the same as in Figs. 2(b)-(e).

can be seen, the bare spin state of middle band does not occur spin flips at the band crossing for conventional doubly [Fig 4(a)] and singly [Fig 4(b)] unpaired TDP, respectively, which is consistent with the results of predicting

topological trivial middle band with $\mathcal{C}_0 = 0$ [Fig 2(b) and 2(c)]. However, the bare spin state of lowest band will occur the spin flips during the crossing process, where double (single) spin flips corresponding the spin angular momentum transition from $|\downarrow\rangle$ ($|0\rangle$) to $|\uparrow\rangle$ ($|\downarrow\rangle$) is connection with topological doubly (singly) TDP with $\mathcal{C} = -2$ ($\mathcal{C} = 1$).

Compared with two types of conventional TDPs, the bare spin state of middle band for unconventional TDPs are observed spin flips process, as shown in Fig. 4(c) and 4(d). Interestingly, Chern number for topological non-trivial middle band is equivalent to changing values of spin angular momentum after spin flips. Analogously, the singly and doubly TDP corresponds single ($|0\rangle \rightarrow |\uparrow\rangle$) and double ($|\uparrow\rangle \rightarrow |\downarrow\rangle$) spin flips for lowest band, respectively. Finally, we should emphasize that the conventional and unconventional unpaired TDPs with their nonzero topological charge can be directly extracted by measurement of spin flips processes along the high-symmetry line in experiment for ultracold atoms [41, 58, 59].

Conclusion.—Based upon the currently available techniques of Raman induced SOC, we proposed an experimental scheme for generating new TDPs for ultracold pseudospin-1 atoms. The phase diagram and band structures have been investigated. It has been shown that the interplay of the quadratic SVMC and STMC gives rise to topological single unpaired TDP and two-fold WPs. In particular, the unconventional singly and doubly TDPs with topological nontrivial middle band are observed. Subsequently, four different types of topologically protected Fermi-arcs states have emerged, linking the unpaired TDP and multiple WPs corresponding the different topological charge. As to the experimental detection, an accessible measurement method to distinguish the different types of TDPs was proposed, which could facilitate the experimental feasibility for studying topological semimetal in cold atoms. Finally, we point out that our scheme can be extended to study exotic topological Fulde-Ferrell superfluid with including collisional interactions in high-spin system [60, 63–65].

This work is supported by the National Key R&D Program of China (Grant No. 2018YFA0307500), the NSFC (Grants No. 11874433, No. 12135018, No. 11874434, and No. 12025509), the Key-Area Research and Development Program of Guangdong Province under Grant No. 2019B030330001, and the Science and Technology Program of Guangzhou (China) under Grant No. 201904020024.

* dengyg3@mail.sysu.edu.cn

† lichaoh2@mail.sysu.edu.cn

[1] N. P. Armitage, E. J. Mele, and A. Vishwanath, “Weyl and Dirac semimetals in three-dimensional solids,” *Rev. Mod. Phys.* **90**, 015001 (2018).

- [2] X. Wan, A. M. Turner, A. Vishwanath, and S. Y. Savrasov, “Topological semimetal and fermi-arc surface states in the electronic structure of pyrochlore iridates,” *Phys. Rev. B* **83**, 205101 (2011).
- [3] A. A. Soluyanov, D. Gresch, Z. Wang, Q. Wu, M. Troyer, X. Dai, and B. A. Bernevig, “Type-II Weyl semimetals,” *Nature(London)* **527**, 495 (2015).
- [4] S. M. Young, S. Zaheer, J. C. Y. Teo, C. L. Kane, E. J. Mele, and A. M. Rappe, “Dirac semimetal in three dimensions,” *Phys. Rev. Lett.* **108**, 140405 (2012).
- [5] D. T. Son and B. Z. Spivak, “Chiral anomaly and classical negative magnetoresistance of Weyl metals,” *Phys. Rev. B* **88**, 104412 (2013).
- [6] X. Huang, L. Zhao, Y. Long, P. Wang, D. Chen, Z. Yang, H. Liang, M. Xue, H. Weng, Z. Fang, X. Dai, and G. Chen, “Observation of the chiral-anomaly-induced negative magnetoresistance in 3D Weyl semimetal TaAs,” *Phys. Rev. X* **5**, 031023 (2015).
- [7] K.-Y. Yang, Y.-M. Lu, and Y. Ran, “Quantum hall effects in a Weyl semimetal: Possible application in pyrochlore iridates,” *Phys. Rev. B* **84**, 075129 (2011).
- [8] A. A. Burkov, “Anomalous hall effect in Weyl metals,” *Phys. Rev. Lett.* **113**, 187202 (2014).
- [9] A. C. Potter, I. Kimchi, and A. Vishwanath, “Quantum oscillations from surface fermi arcs in Weyl and Dirac semimetals,” *Nat. Commun.* **5**, 5161 (2014).
- [10] E. V. Gorbar, V. A. Miransky, I. A. Shovkovy, and P. O. Sukhachov, “Origin of dissipative fermi arc transport in Weyl semimetals,” *Phys. Rev. B* **93**, 235127 (2016).
- [11] Y. Zhang, D. Bulmash, P. Hosur, A. C. Potter, and A. Vishwanath, “Quantum oscillations from generic surface fermi arcs and bulk chiral modes in Weyl semimetals,” *Sci. Rep.* **6**, 23741 (2016).
- [12] S.-Y. Xu, I. Belopolski, N. Alidoust, M. Neupane, G. Bian, C. Zhang, R. Sankar, G. Chang, Z. Yuan, C.-C.g Lee, S.-M. Huang, H. Zheng, J. Ma, D. S. Sanchez, B. Wang, A. Bansil, F. Chou, P. P. Shibayev, H. Lin, S. Jia, and M. Z. Hasan, “Discovery of a Weyl fermion semimetal and topological fermi arcs,” *Science* **349**, 613 (2015).
- [13] L. Lu, Z. Wang, D. Ye, L. Ran, L. Fu, J. D. Joannopoulos, and M. Soljačić, “Experimental observation of Weyl points,” *Science* **349**, 622 (2015).
- [14] B. Q. Lv, H. M. Weng, B. B. Fu, X. P. Wang, H. Miao, J. Ma, P. Richard, X. C. Huang, L. X. Zhao, G. F. Chen, Z. Fang, X. Dai, T. Qian, and H. Ding, “Experimental discovery of Weyl semimetal TaAs,” *Phys. Rev. X* **5**, 031013 (2015).
- [15] Z. K. Liu, B. Zhou, Y. Zhang, Z. J. Wang, H. M. Weng, D. Prabhakaran, S.-K. Mo, Z. X. Shen, Z. Fang, X. Dai, Z. Hussain, and Y. L. Chen, “Discovery of a three-dimensional topological Dirac semimetal Na_3Bi ,” *Science* **343**, 864–867 (2014).
- [16] S. Borisenko, Q. Gibson, D. Evtushinsky, V. Zabolotnyy, B. Büchner, and R. J. Cava, “Experimental realization of a three-dimensional Dirac semimetal,” *Phys. Rev. Lett.* **113**, 027603 (2014).
- [17] Z. K. Liu, J. Jiang, B. Zhou, Z. J. Wang, Y. Zhang, H. M. Weng, D. Prabhakaran, S.-K. Mo, H. Peng, P. Dudin, T. Kim, M. Hoesch, Z. Fang, X. Dai, Z. X. Shen, D. L. Feng, Z. Hussain, and Y. L. Chen, “A stable three-dimensional topological Dirac semimetal Cd_3As_2 ,” *Nat. Mater.* **13**, 677 (2014).
- [18] S.-Y. Xu, C. Liu, S. K. Kushwaha, R. Sankar, J. W.

- Krizan, I. Belopolski, M. Neupane, G. Bian, N. Ali-doust, T.-R. Chang, H.-T. Jeng, C.-Y. Huang, W.-F. Tsai, H. Lin, P. P. Shibayev, F.-C. Chou, R. J. Cava, and M. Z. Hasan, "Observation of fermi arc surface states in a topological metal," *Science* **347**, 294–298 (2015).
- [19] J. Noh, S. Huang, D. Leykam, Y. D. Chong, K. P. Chen, and M. C. Rechtsman, "Experimental observation of optical Weyl points and fermi arc-like surface states," *Nat. Phys.* **13**, 611 (2017).
- [20] Z. Song and X. Dai, "Hear the sound of weyl fermions," *Phys. Rev. X* **9**, 021053 (2019).
- [21] B. Bradlyn, J. Cano, Z. Wang, M. G. Vergniory, C. Felser, R. J. Cava, and B. A. Bernevig, "Beyond dirac and weyl fermions: Unconventional quasiparticles in conventional crystals," *Science* **353**, 5037 (2016).
- [22] Z. Zhu, G. W. Winkler, Q. Wu, J. Li, and A. A. Soluyanov, "Triple point topological metals," *Phys. Rev. X* **6**, 031003 (2016).
- [23] B. Q. Lv, Z.-L. Feng, Q.-N. Xu, X. Gao, J.-Z. Ma, L.-Y. Kong, P. Richard, Y.-B. Huang, V. N. Strocov, C. Fang, H.-M. Weng, Y.-G. Shi, T. Qian, and H. Ding, "Observation of three-component fermions in the topological semimetal molybdenum phosphide," *Nature(London)* **546**, 627 (2017).
- [24] J.-Z. Ma, J.-B. He, Y.-F. Xu, B. Q. Lv, D. Chen, W.-L. Zhu, S. Zhang, L.-Y. Kong, X. Gao, L.-Y. Rong, Y.-B. Huang, P. Richard, C.-Y. Xi, E. S. Choi, Y. Shao, Y.-L. Wang, H.-J. Gao, X. Dai, C. Fang, H.-M. Weng, G.-F. Chen, T. Qian, and H. Ding, "Three-component fermions with surface fermi arcs in tungsten carbide," *Nat. Phys.* **14**, 349 (2018).
- [25] Y. Yang, H.-X. Sun, J.-P. Xia, H. Xue, Z. Gao, Y. Ge, D. Jia, S.-Q. Yuan, Y. Chong, and B. Zhang, "Topological triply degenerate point with double fermi arcs," *Nat. Phys.* **15**, 645 (2019).
- [26] X. Tan, D.-W. Zhang, Q. Liu, G. Xue, H.-F. Yu, Y.-Q. Zhu, H. Yan, S.-L. Zhu, and Y. Yu, "Topological maxwell metal bands in a superconducting qutrit," *Phys. Rev. Lett.* **120**, 130503 (2018).
- [27] X.-Y. Mai, Y.-Q. Zhu, Z. Li, D.-W. Zhang, and S.-L. Zhu, "Topological metal bands with double-triple-point fermions in optical lattices," *Phys. Rev. A* **98**, 053619 (2018).
- [28] H.B. Nielsen and M. Ninomiya, "Absence of neutrinos on a lattice: (i). proof by homotopy theory," *Nucl. Phys.* **B185**, 20 (1981).
- [29] H.B. Nielsen and M. Ninomiya, "Absence of neutrinos on a lattice: (ii). intuitive topological proof," *Nucl. Phys.* **B193**, 173 (1981).
- [30] E. Yukawa, M. Ueda, and K. Nemoto, "Classification of spin-nematic squeezing in spin-1 collective atomic systems," *Phys. Rev. A* **88**, 033629 (2013).
- [31] X.-W. Luo, K. Sun, and C. Zhang, "Spin-tensor-momentum-coupled Bose-Einstein condensates," *Phys. Rev. Lett.* **119**, 193001 (2017).
- [32] Y. Deng, L. You, and S. Yi, "Spin-orbit-coupled Bose-Einstein condensates of rotating polar molecules," *Phys. Rev. A* **97**, 053609 (2018).
- [33] H. Hu, J. Hou, F. Zhang, and C. Zhang, "Topological triply degenerate points induced by spin-tensor-momentum couplings," *Phys. Rev. Lett.* **120**, 240401 (2018).
- [34] H. Hu and C. Zhang, "Spin-1 topological monopoles in the parameter space of ultracold atoms," *Phys. Rev. A* **98**, 013627 (2018).
- [35] Z. Lei, Y. Deng, and C. Lee, "Symmetry-protected topological phase for spin-tensor-momentum-coupled ultracold atoms," *Phys. Rev. A* **102**, 013301 (2020).
- [36] D. Li, L. Huang, P. Peng, G. Bian, P. Wang, Z. Meng, L. Chen, and J. Zhang, "Experimental realization of spin-tensor momentum coupling in ultracold fermi gases," *Phys. Rev. A* **102**, 013309 (2020).
- [37] D.-W. Zhang, Y.-Q. Zhu, Y. X. Zhao, H. Yan, and S.-L. Zhu, "Topological quantum matter with cold atoms," *Advances in Physics* **67**, 253–402 (2018).
- [38] N. R. Cooper, J. Dalibard, and I. B. Spielman, "Topological bands for ultracold atoms," *Rev. Mod. Phys.* **91**, 015005 (2019).
- [39] Y.-J. Lin, K. Jiménez-García, and I. B. Spielman, "Spin-orbit-coupled Bose-Einstein condensates," *Nature (London)* **471**, 83 (2011).
- [40] L. W. Cheuk, A. T. Sommer, Z. Hadzibabic, T. Yefsah, Wa. S. Bakr, and M. W. Zwierlein, "Spin-injection spectroscopy of a spin-orbit coupled fermi gas," *Phys. Rev. Lett.* **109**, 095302 (2012).
- [41] Z. Wu, L. Zhang, W. Sun, X.-T. Xu, B.-Z. Wang, S.-C. Ji, Y. Deng, S. Chen, X.-J. Liu, and J.-W. Pan, "Realization of two-dimensional spin-orbit coupling for Bose-Einstein condensates," *Science* **354**, 83 (2016).
- [42] L. Huang, Z. Meng, P. Wang, P. Peng, S.-L. Zhang, L. Chen, D. Li, Q. Zhou, and J. Zhang, "Experimental realization of two-dimensional synthetic spin-orbit coupling in ultracold fermi gases," *Nat. Phys.* **12**, 540 (2016).
- [43] M. Aidelsburger, M. Atala, S. Nascimbène, S. Trotzky, Y.-A. Chen, and I. Bloch, "Experimental realization of strong effective magnetic fields in an optical lattice," *Phys. Rev. Lett.* **107**, 255301 (2011).
- [44] M. Aidelsburger, M. Atala, M. Lohse, J. T. Barreiro, B. Paredes, and I. Bloch, "Realization of the Hofstadter Hamiltonian with ultracold atoms in optical lattices," *Phys. Rev. Lett.* **111**, 185301 (2013).
- [45] H. Miyake, G. A. Siviloglou, C. J. Kennedy, W. C. Burton, and W. Ketterle, "Realizing the Harper Hamiltonian with laser-assisted tunneling in optical lattices," *Phys. Rev. Lett.* **111**, 185302 (2013).
- [46] G. Jotzu, M. Messer, R. Desbuquois, M. Lebrat, T. Uehlinger, D. Greif, and T. Esslinger, "Experimental realization of the topological Haldane model with ultracold fermions," *Nature(London)* **515**, 237 (2014).
- [47] M. Aidelsburger, M. Lohse, C. Schweizer, M. Atala, J. T. Barreiro, S. Nascimbène, N. R. Cooper, I. Bloch, and N. Goldman, "Measuring the chern number of hofstadter bands with ultracold bosonic atoms," *Nat. Phys.* **11**, 162 (2014).
- [48] C. J. Kennedy, W. C. Burton, W. C. Chung, and W. Ketterle, "Observation of Bose-Einstein condensation in a strong synthetic magnetic field," *Nat. Phys.* **11**, 859 (2015).
- [49] M. Ezawa, "Pseudospin- $\frac{3}{2}$ fermions, type-II weyl semimetals, and critical weyl semimetals in tricolor cubic lattices," *Phys. Rev. B* **94**, 195205 (2016).
- [50] H. Weng, C. Fang, Z. Fang, and X. Dai, "Coexistence of Weyl fermion and massless triply degenerate nodal points," *Phys. Rev. B* **94**, 165201 (2016).
- [51] G. Chang, S.-Y. Xu, B. J. Wieder, D. S. Sanchez, S.-M. Huang, I. Belopolski, T.-R. Chang, S. Zhang, A. Bansil, H. Lin, and M. Z. Hasan, "Unconventional chiral fermions and large topological fermi arcs in \mathbf{RhSi} ," *Phys.*

- Rev. Lett. **119**, 206401 (2017).
- [52] P. Tang, Q. Zhou, and S.-C. Zhang, “Multiple types of topological fermions in transition metal silicides,” *Phys. Rev. Lett.* **119**, 206402 (2017).
- [53] T. Zhang, Z. Song, A. Alexandradinata, H. Weng, C. Fang, L. Lu, and Z. Fang, “Double-Weyl phonons in transition-metal monosilicides,” *Phys. Rev. Lett.* **120**, 016401 (2018).
- [54] H. Gao, Y. Kim, Jörn W. F. Venderbos, C. L. Kane, E. J. Mele, Andrew M. Rappe, and W. Ren, “Dirac-Weyl semimetal: Coexistence of Dirac and Weyl fermions in polar hexagonal *abc* crystals,” *Phys. Rev. Lett.* **121**, 106404 (2018).
- [55] L. Wang and D.-X. Yao, “Coexistence of spin-1 fermion and Dirac fermion on the triangular kagome lattice,” *Phys. Rev. B* **98**, 161403 (2018).
- [56] B. Q. Lv, Z.-L. Feng, J.-Z. Zhao, Noah F. Q. Yuan, A. Zong, K. F. Luo, R. Yu, Y.-B. Huang, V. N. Strocov, A. Chikina, A. A. Soluyanov, N. Gedik, Y.-G. Shi, T. Qian, and H. Ding, “Observation of multiple types of topological fermions in PdBiSe,” *Phys. Rev. B* **99**, 241104 (2019).
- [57] R. Wang, B. W. Xia, Z. J. Chen, B. B. Zheng, Y. J. Zhao, and H. Xu, “Symmetry-protected topological triangular Weyl complex,” *Phys. Rev. Lett.* **124**, 105303 (2020).
- [58] B. Song, C. He, S. Niu, L. Zhang, Z. Ren, X.-J. Liu, and G.-B. Jo, “Observation of nodal-line semimetal with ultracold fermions in an optical lattice,” *Nat. Phys.* **15**, 911 (2019).
- [59] Z.-Y. Wang, X.-C. Cheng, B.-Z. Wang, J.-Y. Zhang, Y.-H. Lu, C.-R. Yi, S. Niu, Y. Deng, X.-J. Liu, S. Chen, and J.-W. Pan, “Realization of an ideal Weyl semimetal band in a quantum gas with 3D spin-orbit coupling,” *Science* **372**, 271–276 (2021).
- [60] Y. Deng, T. Shi, H. Hu, L. You, and S. Yi, “Exotic topological states with Raman-induced spin-orbit coupling,” *Phys. Rev. A* **95**, 023611 (2017).
- [61] “See supplemental material for details about the lattice hamiltonian, the effective hamiltonian for WPs, and calculation of fermi arcs by using surface spectral function.”
- [62] M. P. L. Sancho, J. M. Lopez Sancho, J. M. L. Sancho, and J. Rubio, “Highly convergent schemes for the calculation of bulk and surface green functions,” *J. Phys. F* **15**, 851–858 (1985).
- [63] W. Zhang and W. Yi, “Topological Fulde-Ferrell-Larkin-Ovchinnikov states in spin-orbit-coupled fermi gases,” *Nat. Commun.* **4**, 2711 (2013).
- [64] Y. Cao, S.-H. Zou, X.-J. Liu, S. Yi, G.-L. Long, and H. Hu, “Gapless topological Fulde-Ferrell superfluidity in spin-orbit coupled fermi gases,” *Phys. Rev. Lett.* **113**, 115302 (2014).
- [65] Y. Xu, R.-L. Chu, and C. Zhang, “Anisotropic weyl fermions from the quasiparticle excitation spectrum of a 3D Fulde-Ferrell superfluid,” *Phys. Rev. Lett.* **112**, 136402 (2014).